Comparative Analysis in Drilling Performance of AA7075 in Different Temper Conditions

ESER YARAR (e.yarar@hotmail.com)
Kocaeli Üniversitesi https://orcid.org/0000-0003-1187-5382
Alpay Tamer ERTURK
Kocaeli University
Funda Gül KOÇ
Kocaeli University
Fahri VATANSEVER
Kocaeli University

Research Article

Keywords: AA7075, machining, heat-treatment, thrust force, chip formation, surface roughness, response surface methodology, FEM & FEA

Posted Date: June 29th, 2021

DOI: https://doi.org/10.21203/rs.3.rs-633600/v1

Highlights

- Coverage of the study includes the relationships among the drilling process and microstructure.
- Aspects of the study are evaluations of various temper conditions on drilling performance.
- $MgZn_2$ and secondary particles affect drilling behavior.
- The developed 3D FE model for the drilling process is consistent with the experimental results.

Comparative Analysis in Drilling Performance of AA7075 in Different Temper Conditions

Eser YARAR[a,*], A. Tamer ERTURK[a], Funda Gül KOÇ[b], Fahri VATANSEVER[a]

[a]*Department of Mechanical Engineering, Kocaeli University, Kocaeli, Turkey*
[b]*Department of Metallurgical and Materials Engineering, Kocaeli University, Kocaeli, Turkey*

*Corresponding author: eser.yarar@kocaeli.edu.tr e.yarar@kocaeli.edu.tr (fax +90 2623033003 telephone +90 2623033438)

A B S T R A C T

AA7075 is one of the most suitable materials for aerospace, aircraft, and defense applications with its high yield strength and low-density. In many other modern machining methods, conventional drilling remains the most extensive material removal process in industrial components. The main objective of this study is examining the machinability and surface quality conditions of the AA7075 material with different temper conditions. For this purpose, various temper treatments are implemented to evaluate the impact of microstructural properties on tool wear and surface quality of the drilled holes. The drilling operations have been done on O, F, T4, T6, and T7 temper conditions. Process parameters were three different spindle speeds (715, 1520, and 3030 rev/min) and three feed rates (0.1, 0.2, and 0.3 mm/rev) with HSS-G high-performance ground standard twist drill bit. The present work deals with the effects of temper conditions on thrust force, drilling temperature, tool wear, surface integrity, and chip morphology. Drilling performance is related to the intrinsic microstructural properties of temper conditions. Response surface methodology was used in the evaluation of experiment results. The optimization results showed that while thrust force and torque are not significantly affected by change in spindle speed, they are sensitive to increase in feed rate. Heat-generation on the drill bit is the lowest at low levels of both the feed rate and spindle speed parameters. Among different temper conditions, the AA7075-T6 condition sample is processed with continuous chip formation and resulted in the best hole surface quality. The 3D finite element modelling of the drilling process was carried out, and the drilling performance of AA7075-T6 was evaluated in terms of thrust force, heat generation, and chip formation.

Keywords: AA7075, machining, heat-treatment, thrust force, chip formation, surface roughness, response surface methodology, FEM & FEA

GRAPHICAL ABSTRACT

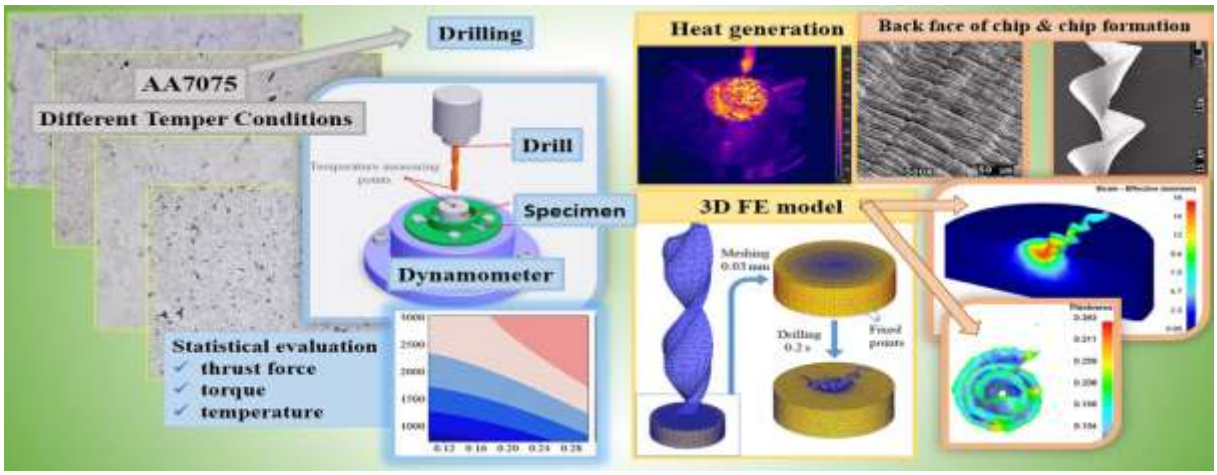

1. Introduction

7xxx series with chromium alloying elements are replacing many structural parts due to the stress corrosion cracking tendency of other series aluminum alloys [1]. AA7075 (Al-Zn-Mg-Cu) is used in aircraft, aerospace, automobile, and transportation industries to make durable and lightweight structural components [2,3]. AA7075 is often used due to its light weight, high strength properties with enhanced fatigue failure characteristics. Post-drilling surface integrity is important for fatigue failure, especially in the use of the aerospace industry. Because drilling causes micro fractures on the hole surface which weaken the material against fatigue failure. A heat-treatment process reconfigures the crystal structure to strengthen alloys mechanical properties. It is important to know that each tempering process gives AA7075 its own distinct characteristics. In general, the main properties of a metallic material affecting machinability are strength properties such as hardness, ductility, and toughness. The machinability status can be improved thanks to changing the mechanical properties as a result of the microstructural design with heat treatment. Zn and Mg alloying elements presents in the AA7075 produce $MgZn_2$ intermetallic phase resulting in an aging treatment, which causes increase in the strength. Drilling with twist drills is the most common operation for various materials types to generate a through-hole in machining and riveting or fastening for many industrial components [3,4]. Aluminum alloys are comparatively soft materials having specific problems in drilling. Surface roughness is the most relevant problem for a metal workpiece in drilling. The industry always aims to process high-quality parts in a short time with faster processing parameters. Besides, surface roughness is greatly affected by the material properties of a workpiece. For this reason, it is necessary to investigate which material condition is more efficient for the machining process.

The drilling process involves two basic operations [3]. The cutting process with the cutting edges of the drill bit, and the extrusion process provided by the helical body of the drill set. After the structural design, the machining of parts in the proper geometry and surface roughness are the main factors in determining the final product quality with proper assembly. Investigation of a drilled hole in terms of quality is made through geometric parameters such as surface roughness, hole form, burr and chip formations. The hole surface quality and burr formation are the frequently encountered problems in the drilling of metallic materials. The most relevant factor affecting surface accuracy in machining is the appropriate selection of the cutting parameters. Therefore, the optimization of the machining parameters is the foremost concern for surface quality. In the drilling process, the hard precipitate components presents in the aluminum alloys and the tendency of plastering due to the ductile character of the material affect

the tool life more than expected [5]. The temperature during the drilling operation is a limiting factor of machining because that tool life decreases with higher temperatures. Also, as the temperature increase has an effect on the mechanical properties of the material such as ductility, it may indirectly affect the hole surface quality. The surface roughness is also important because it is related to the fatigue strength of the end product during its lifetime. The reason for roughness and affecting fatigue life in part machining during drilling is the surface micro-cracks caused by the cutting mechanism [6]. The main parameters affecting the surface quality in the drilling process are the spindle speed, the feed rate of the drill bit, as well as the inclination of the tool to the drilled surface and feed direction. Experiments without statistical methods are insufficient to determine the effect of which parameter on the performance characteristics, and also require a large number of experiments and data. Therefore, several papers have been published on the optimization of cutting parameters in the drilling process. Cakıroglu and Acır investigated drill bit temperature in the drilling process of Al 7075 alloys by using the Taguchi design method [7]. Rajeswari and Amirthagadeswaran studied multiresponse optimization of end milling in aluminum composites using Response Surface Methodology (RSM) based grey relational analysis [8]. Nripen Mondal *et al.* performed regression analysis with satisfactory accuracy for finding optimal conditions in an aluminum alloy drilling [9]. More detailed information about microstructures with various aging treatments can be obtained from a few recent studies for AA7075 alloy [10–12]. There are different studies for AA7075-O in the literature. However, researches for the other temper conditions are very limited [3,13]. Within the scope of this study, heat-treatments used in general industrial applications were performed and microstructures were discussed. The effects of drilling parameters on the formation of chips during the drilling of AA7075 samples were examined. RSM is one of the powerful optimization tools frequently used in experimental research in recent years used to statistically evaluation. This study reports optimize the multiple performance characteristics for different temper conditions in the dry drilling of AA7075. Heat generation detrimentally affects hole quality. Thus, the temperature and the surface roughness were measure and analyze during drilling for each alloy condition. For practical considerations, this article will shed light on the decision at which stage of a production the drilling operation should be performed. Based on the findings presented, manufacturing engineers can decide whether to drill before or after heat treatment application. The finite element method (FEM) was used to comparison and verification test data.

2. Material and Method

2.1. Heat-treatment and microstructural characterization

In this study, the effect of different heat-treatment conditions on the machinability properties of AA7075 series aluminum alloy was investigated. For this purpose, different heat-treatments were applied to the extruded AA7075 specimens with a dimension of Ø25 mm. Table 1 shows the chemical composition of the AA7075 used in this study. Different heat-treatment processes performed on the specimens are given in Table 2.

Table 1. The chemical composition of the investigated AA7075 (wt.%).

	Si	**Fe**	**Cu**	**Mn**	**Mg**	**Zn**	**Cr**	**Ti**	**Al**
This study	0.10	0.22	1.70	0.09	2.51	5.75	0.18	0.02	Bal.
EN 573-3	≤0.40	≤0.50	1.2-2.0	≤0.30	2.1-2.9	5.1-6.1	0.18-0.28	≤0.20	

Table 2. Different heat treatment processes applied to specimens in the study.

Temper	**Process parameters of the heat-treatment**	**Hardness (HV3)**
0	Annealed, the lowest strength, highest ductility temper, 415 °C for 3 h, cooling in the furnace.	65 ± 0.78

F	As fabricated, extrusion rod supplied from the market in T6 condition	190± 1.54
T4	Solution treatment at 480 °C for 3 h, quenching in water at room temperature and natural aging for 72 h.	142.70 ± 1.98
T6	Solution treatment at 480 °C for 3 h, quenching in water at room temperature and artificial aging at 120 °C for 24 h.	188.46 ± 0.73
T7	Solution treatment at 480 °C for 3 h, quenching in water at room temperature and artificial over aging at 165 °C for 24 h.	165.82 ± 2.17

Microstructural investigations were performed using an optical microscope (OM) and Jeol JSM 6060 scanning electron microscope (SEM) with energy-dispersive X-ray spectroscopy (EDX) attachment to observe the changes of microstructure properties obtained due to heat treatment conditions. For this purpose, specimens were polished and etched with Graff Sergeant's solution for the 20s to reveal the microstructure.

Aging conditions have a significant effect on the size, quantity, and distribution of precipitates. During aging treatment, the size and quantity of precipitates increase, initial precipitates are generally coherent, and then becoming semi-coherent, and finally incoherent with the matrix, respectively. The size, distribution, and the coherent degree of precipitates with the matrix have a significant effect on the properties of Al-Zn-Mg-Cu alloys [14–16]. Fig. 1 shows the microstructure of the heat-treated specimens in different conditions. In Fig. 1a, it is seen that the microstructure obtained for the 0 condition contains quite coarse and intermetallics. More homogeneous and fine dispersed $MgZn_2$ (η) precipitates were observed in the microstructure of F and T6 heat treated specimens given in Figs. 1b and d. These precipitates become coarser and non-uniform distributed with T7 heat treatment as seen in Fig. 1e. Also it was seen that precipitation amount of T4 heat treated specimen is less than F, T6 and T7 heat treated specimens accordingly. EDX analysis was performed on specimens to determine the chemical compositions of precipitates observed in the microstructural investigations. According to EDX analysis results given in Fig. 1 while small sized precipitates observed in grain and grain boundaries contain Mg and Zn, coarse precipitates contain Cu, Fe, Mn and Si. $MgZn_2$ is the main precipitate that increases the hardness in AA7075 series aluminum alloy. Coarse Al_2CuMg, AlMnFeSi and Al_7Cu_2Fe precipitates are formed during solidification and cannot be dissolved by solution treatment [17-19].

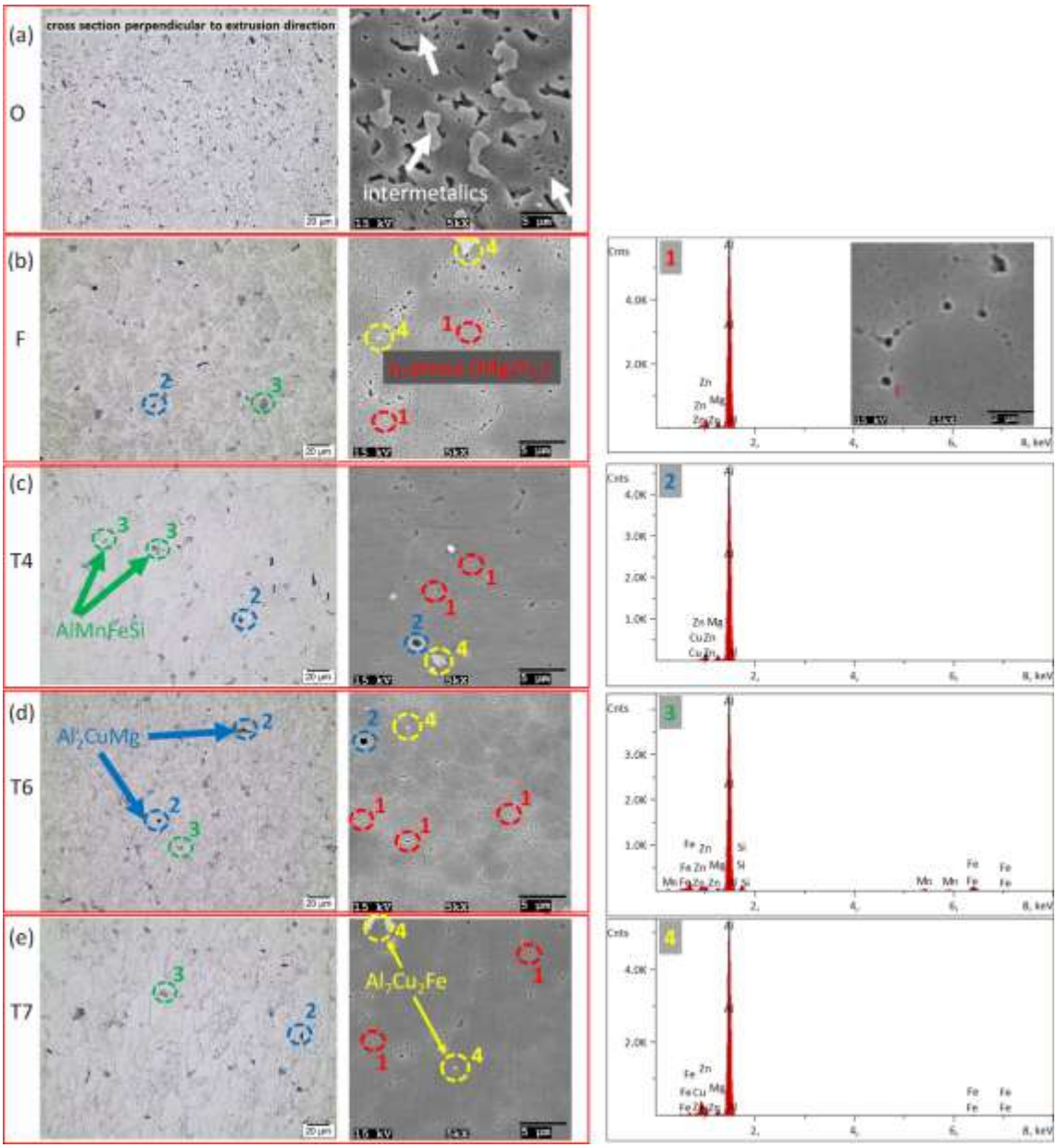

Fig. 1. Microstructures of the heat-treated specimens

Hardness tests were applied by using a Future-Tech Vickers hardness tester under 3 kg load for 10 seconds. Five measurements were carried out for each specimen to have an average value. Hardness values of the heat-treated specimens in different conditions are given in Table 2. High strength and hardness are obtained by reaching the optimum distribution of the fine-sized and high amount of precipitates. Fine and uniform $MgZn_2$ (η) precipitates coherent with matrix lead to an increase in the hardness and strength of 7075 alloys [19]. Hence, the T6 and F heat-treated specimens show the highest material hardness. The lowest material hardness was obtained in the 0 condition specimen as expected. Also, it was seen that T4 condition have lower hardness value when compared with T6 heat-treated specimens. This situation shows that more aging time is required to achieve better properties at T4 heat-treatment conditions. It was observed that the hardness of the specimens decreased as a result of the coarsening in the precipitates due to over aging with T7 heat-treatment.

2.2. Experimental set up, optimization and validation procedure

A Toss United TU5032B vertical drill machine was used in the drilling operations. Experimental set up is provided as a schematic overview in Fig. 2. Each workpiece was rigidly fixed with a specially designed fixture that allows measuring temperature in the machining zone. A Kistler 9272 piezoelectric dynamometer and a 5070A model amplifier were used for cutting force and torque data collection. The data acquisition process is performed utilizing a program called DynoWare by Kistler Co. Drilling temperatures were recorded with a FLIR-A325sc model infrared camera. The infrared camera is placed 50 cm above the workpiece at an angle of 60°. Thus, the measurement can be performed at a drilled hole surface from 5 mm below the upper surface. Temperatures of both drill bit and drilled hole surface were measured one second after the drill bit comes out of the hole. Mean temperatures of the selected areas calculated with the help of FLIR R&D software. A set of three holes were drilled for each combination of input parameters under dry machining condition. During drilling, feeding occurs at Z-direction thus F_x and F_y are practically equal to zero. Thus, F_z is evaluated as the thrust force. The average surface roughness (Ra) is used to evaluate the surface roughness [20,21]. The surface roughness of the inner surface of holes was measured using 2D Mitutoyo SJ-301 measuring device and linearly from the inner surface of each hole and at an angle of 120 ° from three different points. The final surface roughness value was obtained by taking the average of three different measurement results obtained. The geometric characteristics of each hole have been evaluated with SEM and stereo microscope images. Moreover, chip formations were characterized using thermal images obtained from the infrared camera. The various aging treatments of 7075 aluminum alloys in drilling was considered and optimized by conducting drilling experiments using HSS-G high-performance ground standard twist drill, three spindle speeds, three feed rates compared with a response surface methodology (RSM), as seen in Table 3.

Table 3. Selected factors and levels for the DoE model.

Factors	Levels	Values
Workpiece material condition	4	F, T4, T6, T7
Spindle Speed (rev/min)	3	715; 1520; 3030
Feed Rate (mm/rev)	3	0.1; 0.2; 0.3

The full factorial experimental design was employed with the selected parameters. Response Surface Method (RSM) is used to statistically evaluate the effect, significance, and interactions of the independent variables, and the optimal dry drilling parameter settings. The correctness of the model based on analysis of variance (ANOVA) was revealed, and regression equations were acquired with RSM. Four models were established for thrust force, torque, and drill/material temperature. Minitab 19 statistical software was used to evaluate the experimental results. While developing the model, feed rate and spindle speed were defined as continuous, and workpiece material condition as a categorical factor. Here, the 7075-0 condition is not included in the model because its industrial use is quite limited. The relationship between the independent variables and the responses in RSM is defined by a second-order polynomial model given in Eq. 1.

$$y = \beta_0 + \sum_{i=1}^{k} \beta_i x_i + \sum_{i=1}^{k} \beta_{ii} x^2 + \sum_{i=1}^{k-1} \sum_{j=2}^{k} \beta_{ij} X_i X_j + \varepsilon \quad (1)$$

Where y is predicted response, β_0 is constant, β_i, β_{ii} and β_{ij} represent coefficients of linear, quadratic and interaction terms respectively. While X shows the coded variables, ε indicates the error. ANOVA tables, contour and main effect plots were used in the analysis of the

experimental results. ANOVA tables are given in supplementary materials. Test results in the 95% confidence interval for the P values were considered at all variance analysis [21-23].

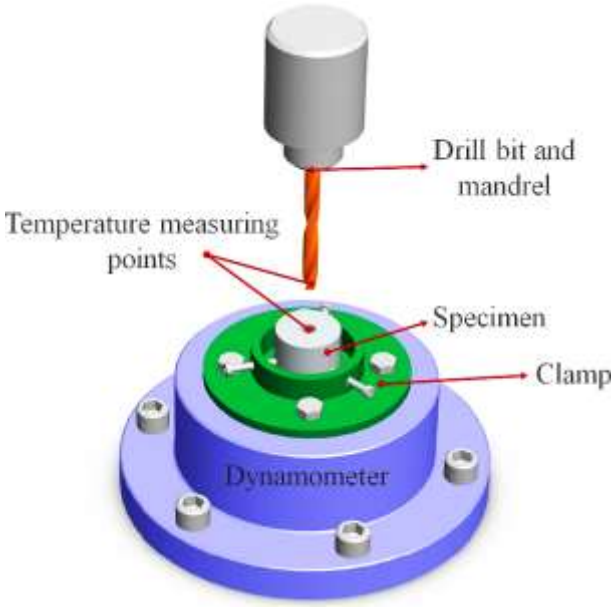

Fig. 2. Experimental setup of the drilling operations.

3. Results

3.1. Evaluation of thrust force and torque

The measurement of forces in the drilling system is essential to investigate the effects of workpiece properties. The resultant force (R) on the lips of the drill bit consists of three components: axial force (F_A), radial force (F_R), and tangential force (F_T). The axial component of the R is also thrust force (F_z) acting on the shear plane during drilling. Besides, the tangential component of the R is also torque (M_z) acting opposite to the direction of rotation. F_z and M_z determine cutting energy for chip creation [21,22]. Figs. 3 and 4 show the main effect and contour plots for thrust force and torque, respectively. From the main effect plots, torque (M_z) and thrust force (F_z) both similarly increased by about 93%, with the increased feed rate from 0.1 to 0.3. The opposite to this, the spindle speed increase resulted in a slight decrease of M_z and F_z. Among the heat treatment types, the differences in F_z obtained varied by up to 10%. Drilling of T6 heat-treated samples resulted in the lowest cutting force value around the mean of 100N.

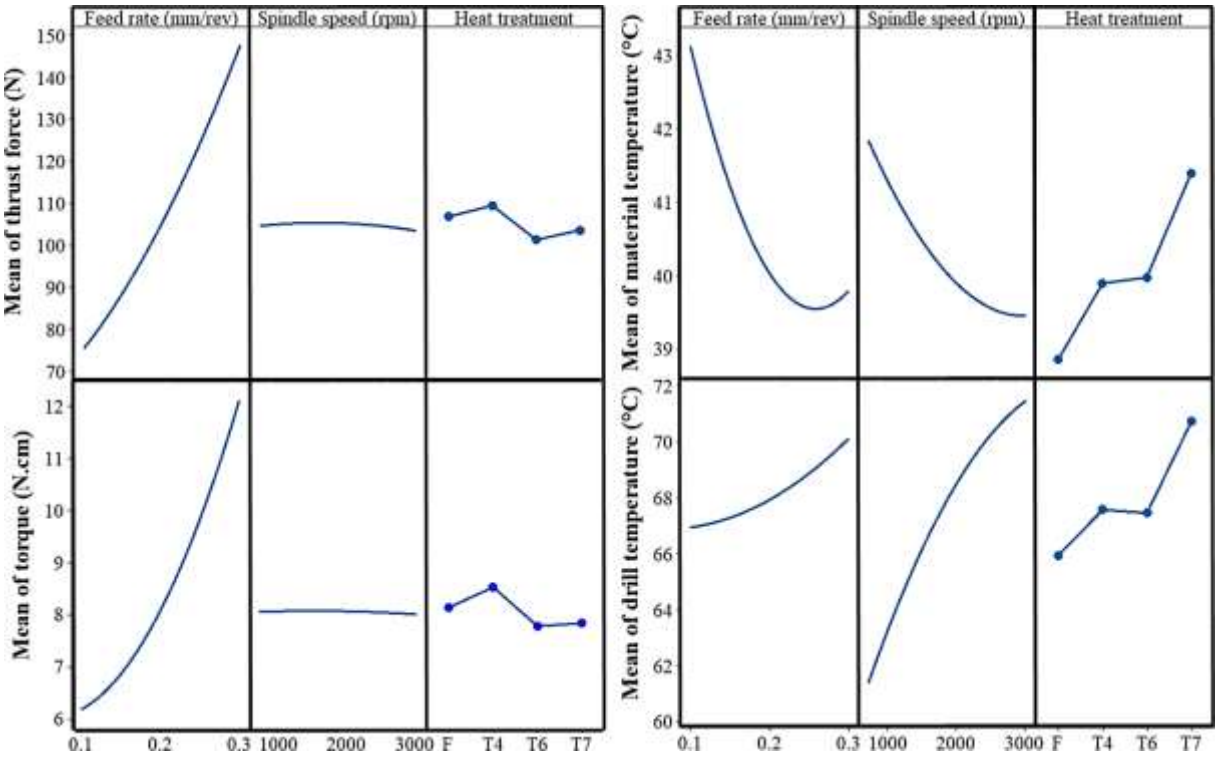

Fig. 3. Main effect plots for thrust force, torque, material, and drill temperature.

Contour graphs obtained depending on the cutting parameters are given in Fig. 4. Increasing the feed rate for each temper condition causes a progressive increase in the cutting force. On the other hand, spindle speed increase shows a rather weak effect, which decreases F_z in the T6 condition and increases in the T7 condition. M_z values increased with increasing feed rate for all heat-treatment conditions. Alternatively, the weak effect of the spindle speed increase in T6 and T7 conditions was also observed for M_z values. As a result, it was seen that the distributions obtained for the cutting torques and forces were compatible with each other.

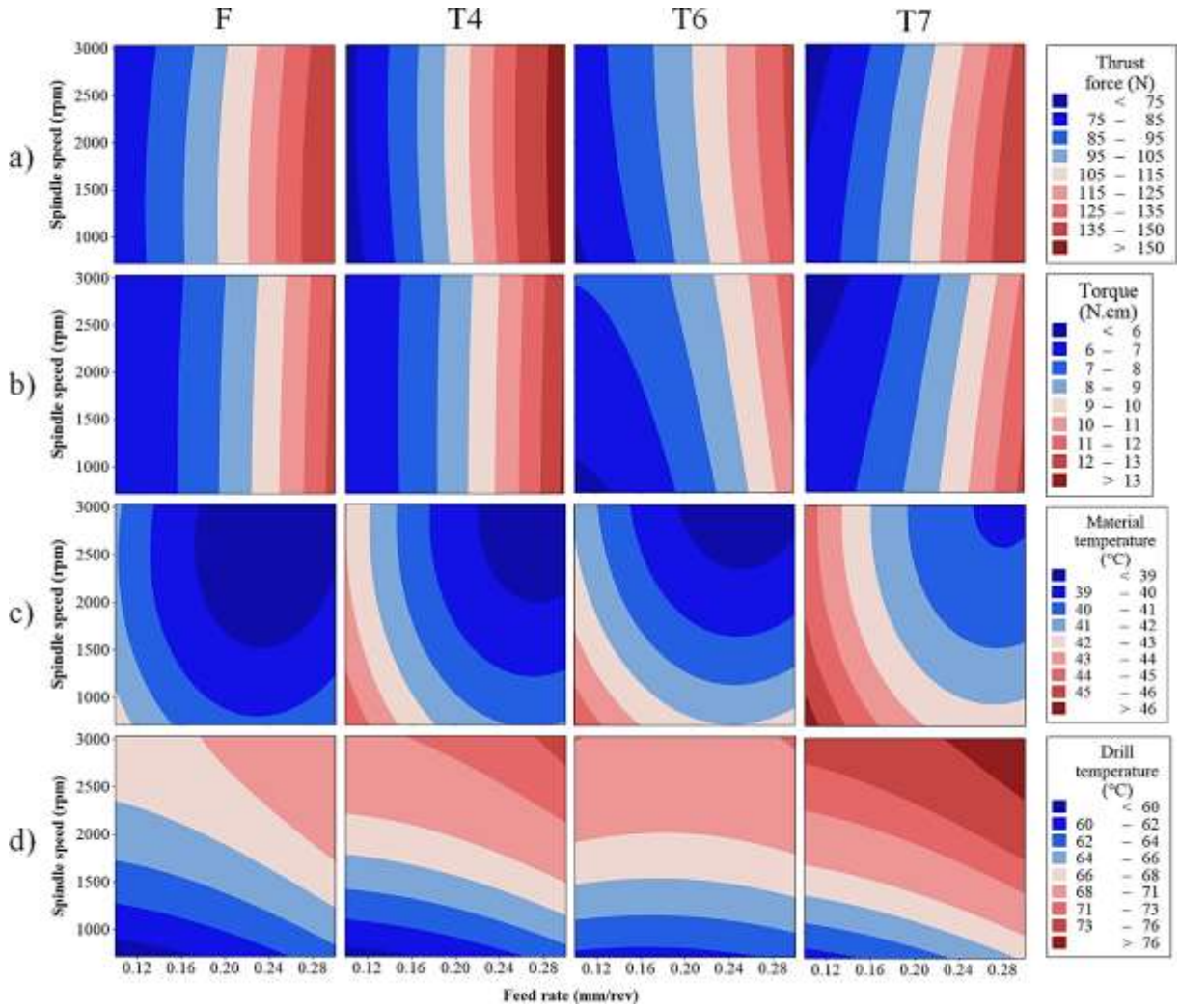

Fig. 4. Contour plots of a) thrust force, b) torque, c) material temperature, and d) drill temperature for different cutting parameters.

3.2. Temperature analyses during drilling operation

The thermo-mechanical effect is decisive in machining of the alloy. The thermo-mechanical effect occurs during material removal processes as plastic deformation of the workpiece and the friction along with the tool-chip interface. The influence that occurred during material removal processes leads to heat generation in the cutting zone. The friction between the workpiece and tool causes the high temperature in the cutting zone. In the machining, most of the heat concentrated in the cutting zone is removed by the chips. The higher temperatures occurred in the cutting zone can significantly shorten the tool life [7]. Therefore, it is substantial to understand how drilling temperatures are affected by the drilling parameters. The amount of generated heat and consequent temperature level of both drill bit and workpiece are desired to know for drilling of samples [21]. The infrared radiation (IR) measuring method gives information about workpiece and tool temperatures. It is possible to monitor moving spindle or drill bit using IR cameras. The main advantage of utilizing an IR camera is to detect temperature distribution around the drilling zone. IR cameras provide another advantage in measuring the average temperature of the selected area. IR cameras are reported as being accurate and reliable [21,24]. The temperatures arising in the drilling process of the tool and workpiece are examined in Figs. 3 and 4, depending on the different heat-treatments applied to AA7075 samples. There is a negligible change of mean 3 °C in terms of the effects of feed rate variables on tool temperature. Spindle speed is a more effective parameter according to the analysis data on the

tool temperature. The difference in spindle speed parameter selection causes an increase of up to 10 °C on the tool temperature. Among the heat-treatment types, samples in the T7 condition have a significant unfavorable effect on tool temperature. Other types of heat treatment, F, T4, and T6, give negligibly different results. As demonstrated by the thermal camera images taken during the drilling operation in Fig. 5, generated heat dissipates by the workpiece, the tool, and chips to the environment. The high thermal conductivity of the AA7075 material contributes to rapid cooling of the specimen by providing heat dissipation.

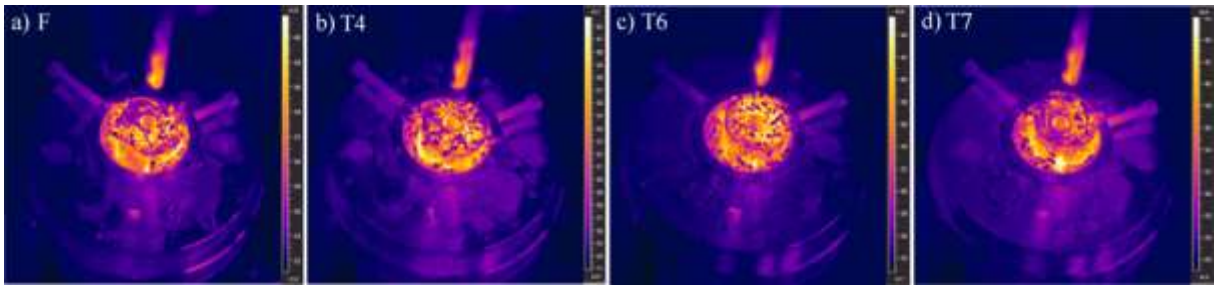

Fig. 5. Heat generation after drilling with 0.1 feed rate and 1520 spindle speed.

Figs. 3 and 4 show the occurred temperatures in the workpiece at different heat treatment conditions during the drilling process, depending on the process parameters. As a result of the increase in parametric level, both of the feed rate and spindle speed factors, there is a slight decrease in the temperature of the workpiece during operation. The occurred temperature in the workpiece for the AA7075-T7 heat treatment condition is higher than the other heat-treatment conditions. T4 and T6 heat-treatments gave similar results on workpiece temperature. However, the specimen in F condition showed the least heating behavior during the drilling process. As a result, temperatures of the hole surface and drill bit are limitedly affected by the difference in heat-treatment type.

3.3. Chip formation and hole surface quality assessment

The ductile and soft properties of non-ferrous alloys make it difficult to drill because of the prolonged contact with the cutting edges of the tool. In machining operations, aluminum alloys exhibit a tendency to adhere to the cutting tool, which leads to build-up edge (BUE) and cutting tool wear. BUE formation in the machining of AA7075 in various heat-treated conditions has been investigated to learn more about the effective mechanism. The BUE is detrimental to surface roughness and dimensional accuracy. According to the temperature investigation, we have presented in the previous section, generated heat has no noticeable effect. Therefore, chip formation and hole surface related to the microstructure and properties of the materials. In this study, since the aluminum alloy composition does not change, two opposite phenomena can dominate the machinability due to the structural differences caused by different heat-treatments. The first fact is that the amount and size of the hard secondary phase in the structure are effective on the abrasive character of the alloy during processing. The second fact is that stacked cutting edge created by adhering to the workpiece makes chip formation and evacuation difficult that results in a detrimental effect on hole geometry and roughness. Which of these two phenomena will be prominent will vary depending on whether the structure originating from heat-treatment has a hard phase or a soft adhesive phase. Intermetallic particles as secondary hard phase can be set in solid solution, grain structure, and dislocations. Forming of the particles as fine strengthening, dispersoid, and constituent role in AA7075 are all changed by the heat-treatment types.

Fig. 6 shows OM images along the drilled holes and SEM images of the hole entry & exit, and a set of images presenting after operation condition of the drill bits for each heat-treatment

conditions. Fig. 6a shows the hole inner surface and tool wear for the 7075-O condition. On the drilled hole entrance and exit examination, the hole gets wider along with the drilling continues. The reason for hole geometry deterioration and the dense deposits of metal plastered on the tool is the adhesion behavior of the soft character of the 7075-O structure during processing. The hole geometry is quite distorted and undesirable compared to other conditions. Moreover, the intermetallics dissolved in the microstructure deformed the inner surface of the hole during cutting due to its brittle and fragile structure. This case indicates that condition O is not suitable for drilling processes. Furthermore, the cutting force was approximately 102 N in this condition. This value is about %25 higher than other temper conditions. Fig. 6b shows deep incision marks in the F condition sample, even at the entrance 0.1 mm/rev. These deep traces have reached half the length of the hole. The entry diameter of the drilled hole is larger. It decreases continuously up to the exit and reaches the minimum. The high hardness and brittle character of the F condition are the most likely reason for these defects. According to the images of the T4 condition in Fig. 6c, there is a notable improvement in hole geometry and BUE compared to the findings in the O condition. We can list these improvements as follows; reduction in deep groove marks at the entry of the hole from OM image, reduction of dimensional difference in hole entry & exit, reduction of the amount of plastered residue on the drill bit cutting edge according to SEM images. The listed improvements are each even more pronounced in T6 heat-treatment sample results in Fig. 6d. In Fig. 6e, entry grooves and accumulation of workpiece material against the rake face in the post-processing images of the T7 heat-treated samples were more damaging than the T6 sample. AA7075 has four types of intermetallic compounds as secondary phases. SEM images in Fig. 1 show the secondary phase distribution for each specimen. The T6 condition exhibits the finer granular η-phases than the T7 sample. Besides, the microstructures of all heat-treatment conditions contain relatively fine AlMnFeSi and coarse Al_2CuMg, Al_7Cu_2Fe precipitates originating from the residual Cu, Fe, and Si element. Soaking time and annealing temperature, which are heat-treatment variables, are the main factors in microstructure formation. Reportedly, annealing applications reduce yield strength and improved tensile elongation compared to as-received AA7075 materials. According to the knowledge obtained from previous studies, fine secondary particles do not show deformation in the tensile test and have limited influences on the overall structure in terms of deformation mechanism. It has also been reported that lattice turns are limited nearby the thin secondary phases. In contrast, coarse secondary particles deformed and showed a fracture [25,26]. Grains with coarse secondary particles would exhibit an easy slip system and transformed strain through the slip bands, which promote deep incision marks and sticky BUE formation in the F and T6 condition samples. During the cutting process, the coarse secondary particles underwent tear and separation.

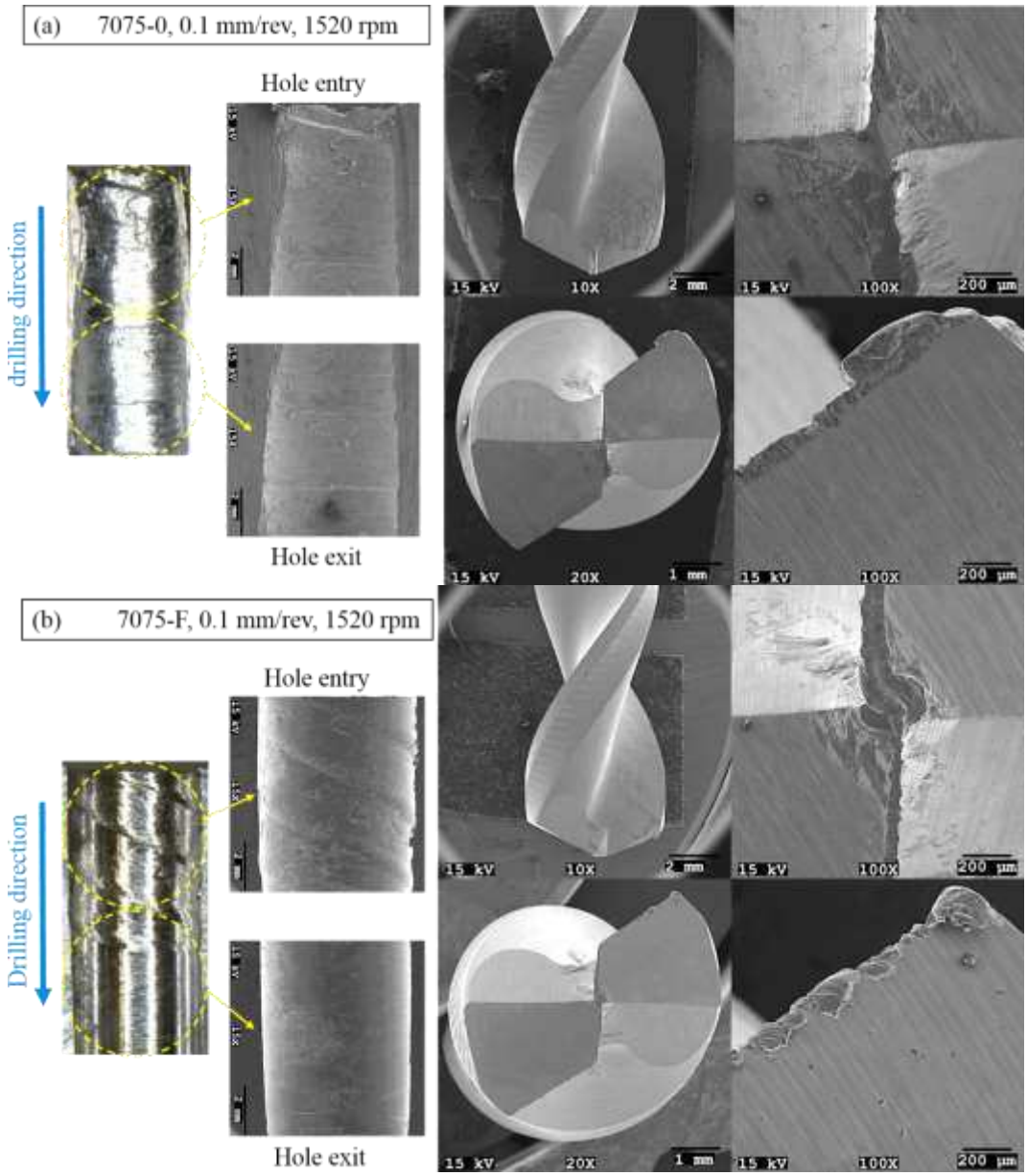
(a) 7075-0, 0.1 mm/rev, 1520 rpm
Hole entry
drilling direction
Hole exit
15 kV 10X 2 mm
15 kV 100X 200 µm
15 kV 20X 1 mm
15 kV 100X 200 µm
(b) 7075-F, 0.1 mm/rev, 1520 rpm
Hole entry
Drilling direction
Hole exit
15 kV 10X 2 mm
15 kV 100X 200 µm
15 kV 20X 1 mm
15 kV 100X 200 µm

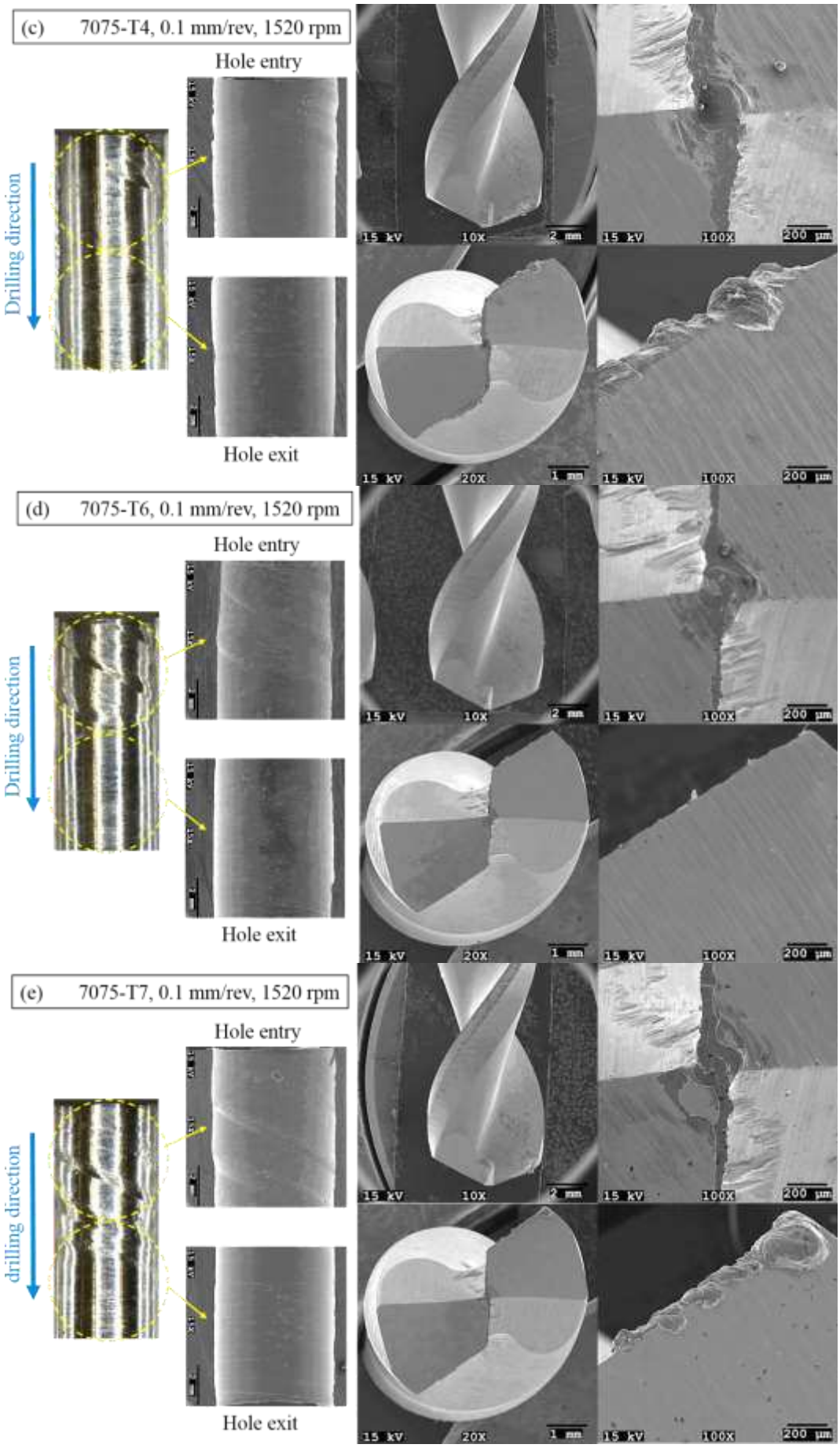
(c) 7075-T4, 0.1 mm/rev, 1520 rpm
Hole entry
Drilling direction
Hole exit
(d) 7075-T6, 0.1 mm/rev, 1520 rpm
Hole entry
Drilling direction
Hole exit
(e) 7075-T7, 0.1 mm/rev, 1520 rpm
Hole entry
drilling direction
Hole exit

Fig. 6. A set of selected micrographs for evaluating the BUE and hole formations.

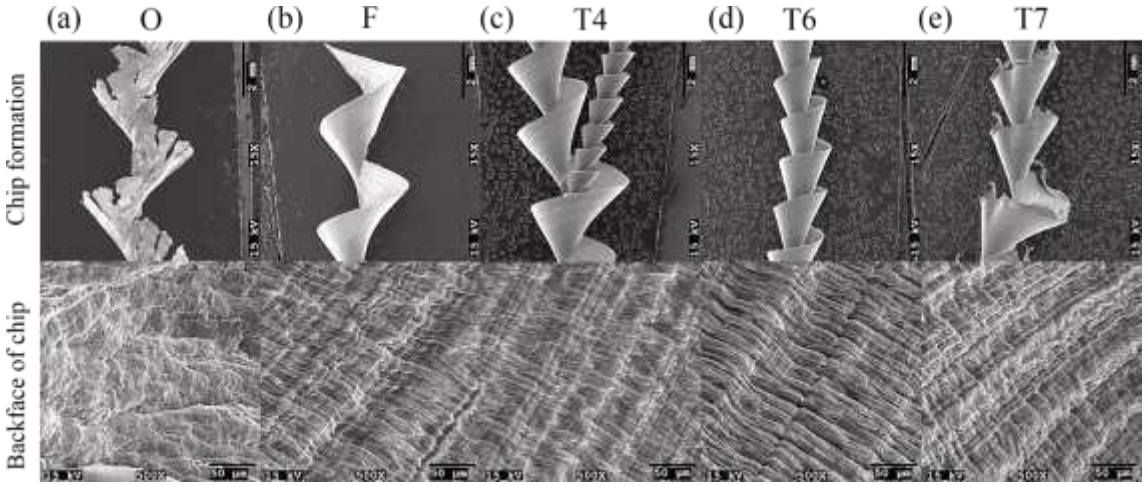

Fig. 7. Chip formations for various heat-treatment conditions (0.1 mm/rev, 1520 rpm).

In Fig. 7, different chip formations obtained in experiments conducted under the same cutting parameters (0.1 mm/rev, 1520 rpm) are presented. While deformed chip morphology occurs in Fig. 7a, there are relatively fewer differences among other chip structures. The lower strength, hardness, and high ductility properties of the AA7075-O sample made the chip flow irregular during drilling. The material that needs to be removed in the form of chips tends to stick to the drill rather than thrown out, and the chip structure quickly deteriorates. In addition, coarse intermetallics in the microstructure provided fragility during cutting and negatively affected the plastic deformation mechanism in chip formation. As a result, the uneven chip flow deforms the hole's inner surface and increases the cutting forces. Besides, the chip formations that occur in Figs. 7b and d are in continuous form and spiral structure. Continuous chip structure occurs at lower feed rates and in the processing of relatively ductile metals such as aluminum. This chip structure adheres to the tool and causes BUE formation [20]. BUE formation is observed for each temper condition in Fig. 6. Among the chip structures, the F and T6 conditions have the most desirable chip form. It is thought that $MgZn_2$ precipitates, which display a finer and homogeneous distribution in the microstructure, provide an advantage during cutting. In Fig. 7c, it is seen that chip formation begins in a new flat helical form before the conical spiral chip formation ends [23]. In T4 heat treatment, the chip structure can be formed in a different form, as it cannot reach the sufficient precipitate density and therefore the maximum hardness. In Fig. 7e, a relatively damaged continuous spiral chip formation is seen. Because the grain structure, which became coarse due to over-aging, decreased the hardness, increased the efficiency of the secondary phases in the microstructure, and deformed the chip structure.

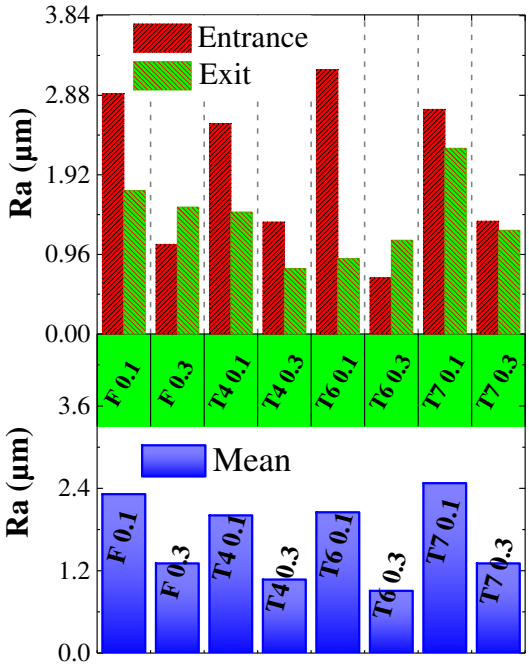

Fig. 8. Effects of the feed rate on the surface roughness (1520 rpm).

It is crucial to obtain a smooth surface in industrial applications because the rough surfaces generally wear faster. Sliding contact of rough surfaces has a higher friction coefficient than smooth surfaces. Surface quality mostly depends on chip formation and environmental conditions. The point angle of a drill bit does not affect chip removal rate, but the cross-sectional area of a non-deformed chip affects uncut chip thickness and width [20]. In the current study, the drilling behavior of heat-treated materials is revealed in the drilling process performed by keeping the point angle of 118° constant. This point angle is the 'standard' angle for most drills used in industrial applications [27].

Fig. 8 shows that the change in feed rate affects average surface roughness. The surface roughness measurement was separately performed at the hole entry and exit. For each temper condition, the roughness level at the hole entry is higher than the hole exits. This situation can be observed from the images of the hole inner surface given in Fig. 6. The helical traces observed in the figure increased the roughness at the hole's entrance. These tracks diminished towards the hole exit because of adhesive wear at the cutting edges of the drill bit. As a result, this situation caused narrower hole exit geometry. It is also determined that the T6 temper condition has the lowest average roughness. The high strength of T6 has facilitated chip formation and flow. Thus, higher surface quality occurred. The chip structure given in Fig. 7d for T6 has the desired helical and undeformed structure for drilling processes. On the other hand, the highest roughness value was obtained for the T7 temper condition according to Fig. 8. Continuous contact of the drill bit with the inner surface of the hole heats the drill and the workpiece, which increases the ductility and deformations of the drilled hole, resulting in higher surface roughness [28]. As can be seen in Fig. 3, the highest cutting temperatures were obtained for the T7 temper condition. The chip structure in Fig. 7e also explains occurring the roughest surface in the T7 temper condition. In general, the drilled holes become smoother with the increase of the feed rate. Considerably, feed rate in 0.3 mm/rev gives better surface roughness.

3.4. Regression equations

The regression equations given in Table 4 for thrust force, torque, material, and drill temperature were experimentally derived with the use of regression analysis and analysis of

variance (ANOVA). Here, the coefficients of linear, interaction, and quadratic terms are presented separately for each response. The ability of the regression equations to estimate the test results is expressed by the R^2. Predicted R^2 shows the ability of prediction of possible new observations with the obtained regression equation [29]. R^2 and R^2 (pred.) values obtained for each response are given in Table 4. Accordingly, the statistical model has a high enough ability to predict the simulation results.

Table 4. Empirical models of drilling operation responses.

		Constant	F	S	F^2	S^2	F.S
Thrust force (N)	F =	59.31	108.8	0.00293	622	-0.000001	-0.00361
	T4 =	41.41	193.2	0.00487	622	-0.000001	-0.00361
	T6 =	56.74	59.4	0.00662	622	-0.000001	-0.00361
	T7 =	59.45	114.9	0.0005	622	-0.000001	-0.00361
R^2= 96.47% R^2(pred.)= 95.39%							
Torque (N.cm)	F =	5.99	-10.62	0.000169	107.5	0	-0.00067
	T4 =	5.58	-6.85	0.000196	107.5	0	-0.00067
	T6 =	6.04	-17.89	0.000731	107.5	0	-0.00067
	T7 =	6.82	-12.92	-0.000191	107.5	0	-0.00067
R^2= 89.29% R^2(pred.)= 85.77%							
Mat. Temp. (°C)	F =	48.97	-64.52	-0.002153	142.92	0	-0.001384
	T4 =	52.683	-75.54	-0.002403	142.92	0	-0.001384
	T6 =	52.345	-68.57	-0.002924	142.92	0	-0.001384
	T7 =	54.474	-76.38	-0.002467	142.92	0	-0.001384
R^2= 96.18% R^2(pred.)= 94.80%							
Drill. Temp. (°C)	F =	53.38	-1	0.00796	60.6	-0.000001	-0.00173
	T4 =	52.97	-3.5	0.00932	60.6	-0.000001	-0.00173
	T6 =	57.39	-18.5	0.0085	60.6	-0.000001	-0.00173
	T7 =	53.89	2.6	0.00987	60.6	-0.000001	-0.00173
R^2= 93.21% R^2(pred.)= 90.85%							

** F: Feed rate, S: Spindle Speed, D: HSS G*

3.5. 3D FE model of the drilling process

In this section, the drilling process of 7075 aluminum alloy is modeled using Deform 3D software. 3D computational modeling is utilized to predict chip formation, thrust force, and temperature. Based on the experimental results, the drilling process was modeled for 7075-T6 alloy and feedrate of 0.1 mm/rev and 1520 rpm, considering that T6 alloy gives the most optimum and effective results. There are modeling studies for 7075-T6 alloy using different Johnson-Cook material models in the literature [30,31]. In this study, the tabular data format containing strain, strain rate and temperature measurements with a larger scale measured separately was used. Tabular data format in the Deform 3D library was selected to define the mechanical and thermal properties of AA7075-T6.

$$\bar{\sigma} = (\bar{\varepsilon}, \dot{\bar{\varepsilon}}, T) \quad (2)$$

Where $\bar{\sigma}$ is flow stress, $\bar{\varepsilon}$ is effective plastic strain, $\dot{\bar{\varepsilon}}$ is effective strain rate, and T is temperature. This model is suitable for the drilling process as it defines the flow behavior as a function of strain, strain rate, and temperature. Other mechanical and thermal properties used in modeling are given in Table 5. The logarithmic interpolation method was chosen as the interpolation method. The implicit Lagrangian computational routine was used to simulate the drilling process and the distorted elements of the mesh with continuous adaptive remeshing [32]. The workpiece and drill were defined as a plastic and rigid body, respectively [33]. The frictional condition was defined as the constant shear friction factor, m = 0.7, between the aluminum workpiece-drill interface [31]. The workpiece has meshed into nearly 1.5×10^5 tetrahedron elements with a minimum element size of 0.03 mm and the high-density mesh was placed at the drilling zone. The tetrahedron element type can be efficiently used in plastic deformation simulations [34]. Similarly, the drill bit was discretized into 1×10^4 tetrahedron elements with higher mesh density in the drilling contact zone. The 3D FE model of the drilling process is shown in Fig. 9.

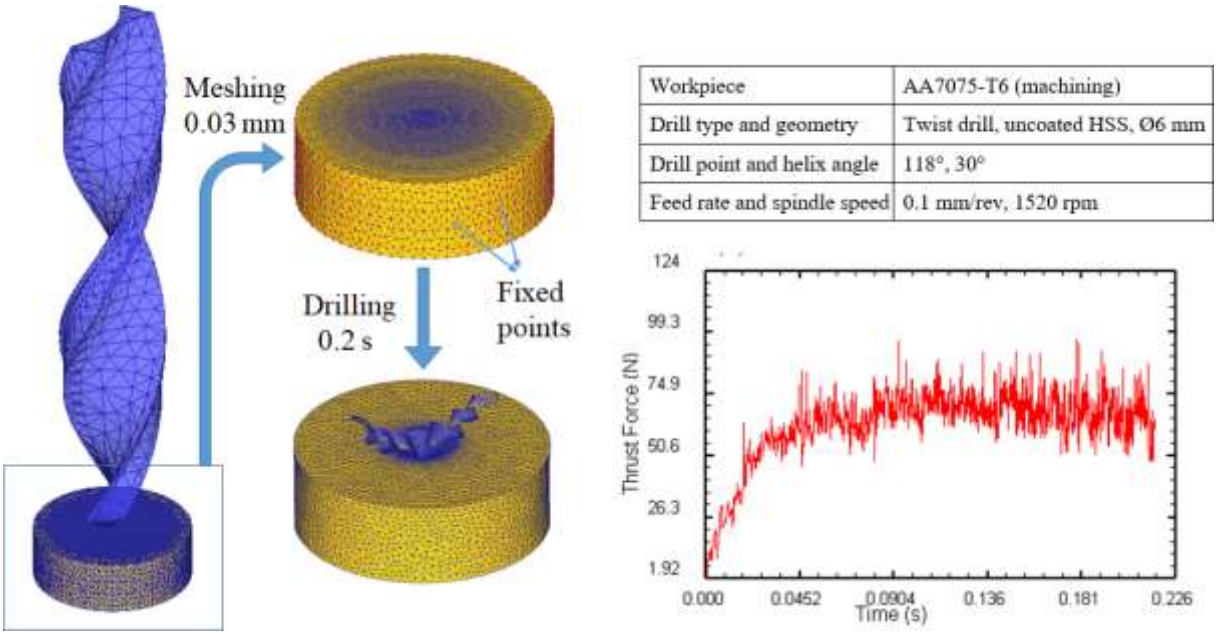

Fig. 9. 3D FE model of drilling procedure and thrust force graph.

The thrust force graph obtained after the simulation is also given in Fig. 9. Accordingly, thrust force was found about 71.62 N. This value predicts the experimental thrust force data under the same parameters with an error of 4.62%, which is an insignificant difference. Consequently, it was observed that the developed 3D model for the drilling process is consistent with the experimental results.

Table 5. Mechanical and thermal properties of workpiece used in FE simulations.

Properties	AA7075-T6
Thermal conductivity, (N sec^{-1} $°C^{-1}$)	180.175
Heat capacity, (N mm^{-2} $°C^{-1}$)	2.43369
Thermal expansion coefficient, ($°C^{-1}$)	2.2E-05
Young's modulus, (GPa)	68.9
Poisson's ratio	0.3

Fig. 10 shows the temperature, effective stress, and effective strain distributions occurring on the workpiece during drilling. Accordingly, the maximum effective strain and stress values

were found to be ~ 16 (mm/mm) and ~ 790 MPa, respectively. After the regular chip flow started, the maximum stress and strain values have remained at these values throughout the simulation until the chip formation reached the conical structure. Similarly, the temperature in the contact zone was found to be about 40-45 °C. In Fig. 12, the temperature change graph of the P1 point selected from the center of the workpiece is given during the simulation. Accordingly; the temperature increase of the P1 point has continued until about 50-55 °C and then a decreasing trend has begun. It is seen that the heat generated during cutting is removed from the workpiece by chip. In addition, it is seen that the predicted temperature values are in accordance with those given in Fig. 5c.

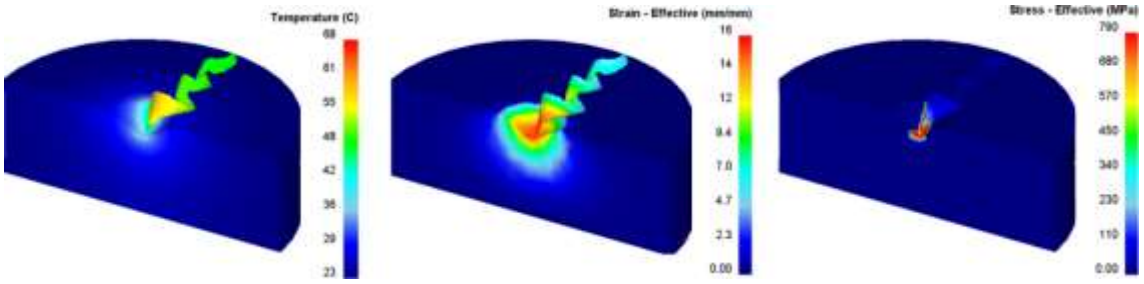

Fig. 10. Predicted temperature, strain and stress distributions in the chip and workpiece (AA7075-T6, 0.1 mm/rev, 1520 rpm)

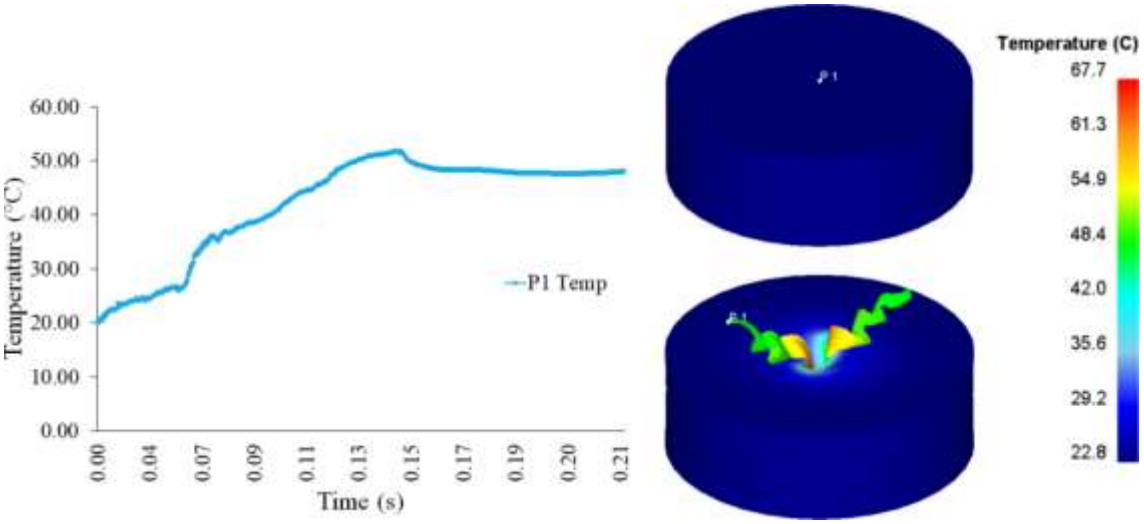

Fig. 11. Predicted temperature distribution for the P1 point.

The thrust force and temperature distribution obtained in the simulation so far are compatible with the experimental data. These data are decisive for parameters affecting chip formation. This conformity is expected to be in harmony with the chip structure during drilling. In Fig. 12, chip structures obtained both in experimental and simulation are given. At first glance, it is striking that the chip structure formed in the simulation is almost the same as that obtained in the experiment. One of the parameters used to compare chip formations is chip thickness [31,35]. The chip thicknesses obtained in the experiment were measured using an OM. On the chip thicknesses comparing, the experimental results are in perfect agreement with the simulation results. As a result, the 3D model developed for AA7075-T6 is extremely consistent in terms of temperature, force, and chip structures.

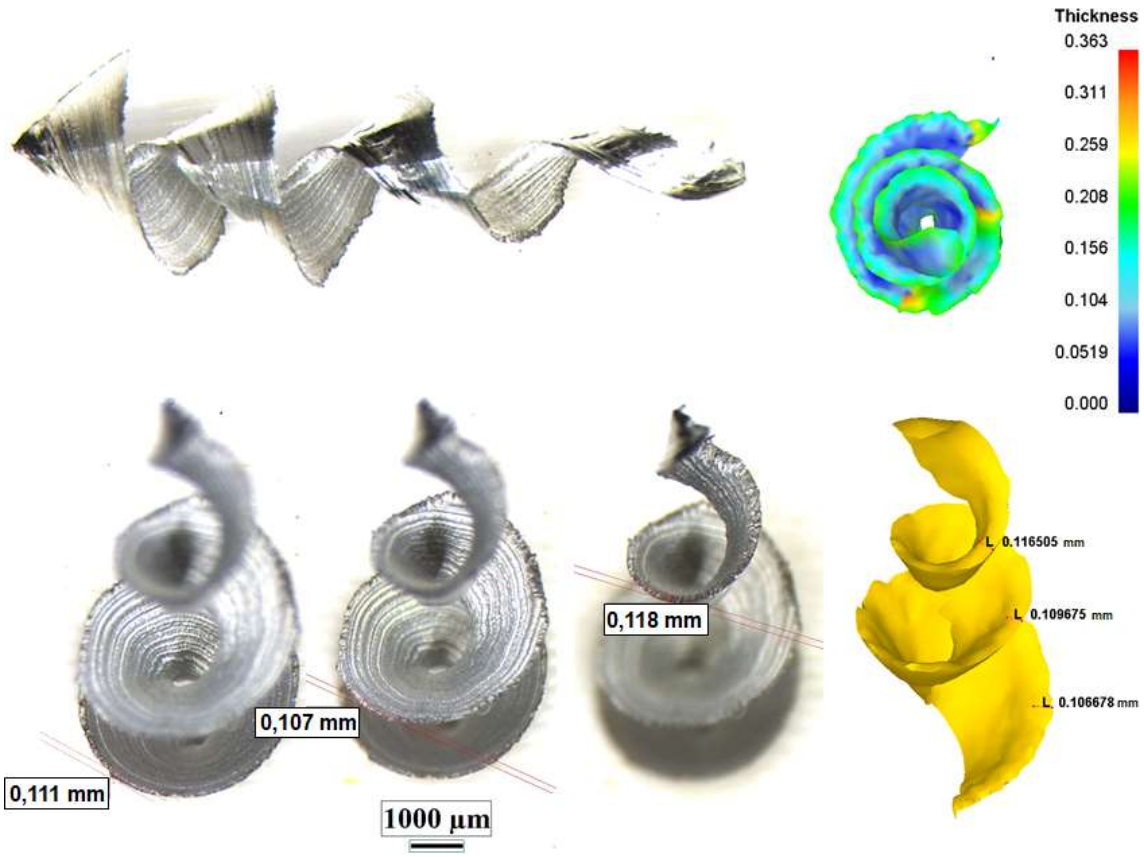

Fig. 12. Comparison of chip formation obtained in simulation and experiment (AA7075-T6, 0.1 mm/rev, 1520 rpm)

Conclusions

In this work, the effect of heat-treatment features on drilling behaviors and chip formation mechanisms of AA7075 was investigated. The following conclusions can be drawn:

- According to the thrust force and torque results, M_z and F_z both similarly increased by about 93%, with the increased feed rate. The spindle speed increase resulted in a slight decrease of M_z and F_z from the main effects and counterplots. F_z varies up to 10%, according to the temper conditions.
- Tool temperature exhibits a little change with feed rate while spindle speed differences cause up to 10 °C increasings. Temper conditions put on a negligible effect on workpiece temperature during the drilling operation owing to the high thermal conductivity of the AA7075 material. The T7 condition samples had a distinct adverse effect on the tool temperature.
- Chip formation and hole surface quality are related to the microstructure rather than heat generation. It is thought that $MgZn_2$ precipitates, which display a finer and homogeneous distribution in the microstructure, provide an advantage during cutting.
- The F and T6 condition samples resulted in deep incision marks up to half the hole length. Thus, the entry diameters are larger than the exit. The T7 temper condition revealed entry grooves and accumulation against the rake face and exhibited more damaging character than the T6 samples.
- Chip formation of O condition sample tends to stick to the drill and deformed form. The T7 sample results in a damaged continuous spiral form, while the F and T6 conditions have the most desirable chip formation.

- The regression equations for estimating the test results have a high enough ability to predict the simulation results.
- There is good agreement between the experimental and computational analysis for chip formation, thrust force, and temperature distribution. Chip formations are very similar to each other.
- T6 heat-treatment makes AA7075 much stronger, but this extra strength is negligible and a cause of cost increase in many applications. In this study, we drilled holes without natural aging immediately after T6 heat treatment in the laboratory. The naturally aged material from the market was also drilled for comparison. There was a slight difference in the cutting force of 10N between them. Therefore, it is not technically necessary to re-apply T6 to naturally aged raw materials for the drilling procedure. It is also not economical. If mass production is made and there are special requirements in terms of hole character, drilling operation immediately after T6 is applied stands out as advantageous in terms of tool life and indirect costs.

Acknowledgment
The authors thank the Advanced Material Laboratory at Kocaeli University Technopark for supporting our experiments.

Author contribution Eser Yarar: conceptualization, methodology, validation, writing, simulation, and optimization. Alpay Tamer Ertürk: review, conceptualization, methodology, validation, writing-review and editing. Funda Gül Koç: review, conceptualization, methodology, materials characterization, writing-review and editing Fahri Vatansever: review, conceptualization, methodology, validation, writing-review and editing

Data availability All data generated or analyzed during this study are included in this published article, and further request can be contacted with the corresponding author.

Funding This study was supported by Kocaeli University Scientific Research Projects Coordination Unit. Project Number: FHD-2020-1579.

Declarations

Ethical approval Not applicable
Code availability Not applicable
Consent to participate Not applicable
Consent for publication Not applicable
Competing interests The authors declare no competing interests.

References

[1] Das D, Prasanna Sahoo B, Bansal S, Mishra P. Experimental investigation on material removal rate and chip forms during turning T6 tempered Al 7075 alloy. Mater Today Proc 2018;5:3250–6. https://doi.org/10.1016/j.matpr.2017.11.566.
[2] Köklü U. Influence of the process parameters and the mechanical properties of aluminum alloys on the burr height and the surface roughness in dry drilling. Mater Tehnol 2012;46:103–8.
[3] Kao JY, Hsu CY, Tsao CC. Experimental study of inverted drilling Al-7075 alloy. Int J Adv Manuf Technol 2019;102:3519–29. https://doi.org/10.1007/s00170-019-03416-8.
[4] Bahçe E, Özdemir B. Investigation of the burr formation during the drilling of free-form surfaces in al 7075 alloy. J Mater Res Technol 2019;8:4198–208.

https://doi.org/10.1016/j.jmrt.2019.07.028.
[5] Coldwell HL, Dewes RC, Aspinwall DK, Renevier NM, Teer DG. The use of soft/lubricating coatings when dry drilling BS L168 aluminium alloy. Surf Coatings Technol 2004;177–178:716–26. https://doi.org/10.1016/j.surfcoat.2003.08.012.
[6] Sedighi M, Nasrollahi M, Joudaki J. Surface integrity in broaching of AA 7075-T651 aluminum alloys. Mach Sci Technol 2019;23:79–94. https://doi.org/10.1080/10910344.2018.1466329.
[7] Çakiroğlu R, Acir A. Optimization of cutting parameters on drill bit temperature in drilling by Taguchi method. Meas J Int Meas Confed 2013;46:3525–31. https://doi.org/10.1016/j.measurement.2013.06.046.
[8] Rajeswari B, Amirthagadeswaran KS. Experimental investigation of machinability characteristics and multi-response optimization of end milling in aluminium composites using RSM based grey relational analysis. Meas J Int Meas Confed 2017;105:78–86. https://doi.org/10.1016/j.measurement.2017.04.014.
[9] Mondal N, Mandal S, Mandal MC. FPA based optimization of drilling burr using regression analysis and ANN model. Meas J Int Meas Confed 2020;152:107327. https://doi.org/10.1016/j.measurement.2019.107327.
[10] LI J feng, PENG Z wei, LI C xing, JIA Z qiang, CHEN W jing, ZHENG Z qiao. Mechanical properties, corrosion behaviors and microstructures of 7075 aluminium alloy with various aging treatments. Trans Nonferrous Met Soc China (English Ed 2008;18:755–62. https://doi.org/10.1016/S1003-6326(08)60130-2.
[11] Atkinson H V., Burke K, Vaneetveld G. Recrystallisation in the semi-solid state in 7075 aluminium alloy. Mater Sci Eng A 2008;490:266–76. https://doi.org/10.1016/j.msea.2008.01.057.
[12] Vatansever F, Erturk AT, Feyzullahoglu E. Effect of ultrasonic melt treatment on the tribological behavior of 7075 aluminum alloy. Mater Test 2020;62:1243–50. https://doi.org/10.3139/120.111610.
[13] Kilickap E. Modeling and optimization of burr height in drilling of Al-7075 using Taguchi method and response surface methodology. Int J Adv Manuf Technol 2010;49:911–23. https://doi.org/10.1007/s00170-009-2469-x.
[14] Zang JX, Zhang K, Dai SL. Precipitation behavior and properties of a new high strength Al-Zn-Mg-Cu alloy. Trans Nonferrous Met Soc China (English Ed 2012;22:2638–44. https://doi.org/10.1016/S1003-6326(11)61511-2.
[15] Isadare AD, Aremo B, Adeoye MO, Olawale OJ, Shittu MD. Effect of heat treatment on some mechanical properties of 7075 Aluminium alloy. Mater Res 2013;16:190–4. https://doi.org/10.1590/S1516-14392012005000167.
[16] Rometsch PA, Zhang Y, Knight S. Heat treatment of 7xxx series aluminium alloys - Some recent developments. Trans Nonferrous Met Soc China (English Ed 2014;24:2003–17. https://doi.org/10.1016/S1003-6326(14)63306-9.
[17] Guo W, Guo J, Wang J, Yang M, Li H, Wen X, Zhang J, volution of precipitate microstructure during stress aging of an Al-Zn-Mg-Cu alloy. Mater Sci Eng A.2015;634:167-175. https://doi.org/10.1016/j.msea.2015.03.047.
[18] Hua L, Hu X, Han X. Microstructure evolution of annealed 7075 aluminum alloy and its influence on room-temperature plasticity. Mater Des 2020;196:109192. https://doi.org/10.1016/j.matdes.2020.109192.
[19] Koç FG, Çöl M, Çeliker T. Effect of cooling rate on microstructure, mechanical properties and residual stress of 7075 aluminum alloy. Mater Test 2018;60:989–96. https://doi.org/10.3139/120.111242.
[20] Aamir M, Giasin K, Tolouei-Rad M, Vafadar A. A review: drilling performance and hole quality of aluminium alloys for aerospace applications. J Mater Res Technol

2020;9:12484–500. https://doi.org/10.1016/j.jmrt.2020.09.003.
[21] Erturk AT, Vatansever F, Yarar E, Guven EA, Sinmazcelik T. Effects of cutting temperature and process optimization in drilling of GFRP composites. J Compos Mater 2020. https://doi.org/10.1177/0021998320947143.
[22] Erturk AT, Vatansever F, Yarar E, Karabay S. Machining behavior of multiple layer polymer composite bearing with using different drill bits. Compos Part B Eng 2019;176. https://doi.org/10.1016/j.compositesb.2019.107318.
[23] Yarar E, Karabay S. Investigation of the effects of ultrasonic assisted drilling on tool wear and optimization of drilling parameters. CIRP J Manuf Sci Technol 2020. https://doi.org/10.1016/j.cirpj.2020.06.002.
[24] Dörr J, Mertens T, Engering G, Lahres M (2003) "In-situ" temperature measurement to determine the machining potential of different tool coatings. Surf Coatings Technol 174–175:389–392. https://doi.org/10.1016/S0257-8972(03)00708-4
[25] Liu C, Liu Y, Ma L, Yi J. Effects of solution treatment on microstructure and high-cycle fatigue properties of 7075 aluminum alloy. Metals (Basel) 2017;7. https://doi.org/10.3390/met7060193.
[26] Hua L, Hu X, Han X. Microstructure evolution of annealed 7075 aluminum alloy and its influence on room-temperature plasticity. Mater Des 2020;196:109192. https://doi.org/10.1016/j.matdes.2020.109192.
[27] Astakhov VP. 2 - Drilling. In: Paulo Davim J, editor. Mod. Mach. Technol., Woodhead Publishing; 2011, p. 79–212. https://doi.org/https://doi.org/10.1533/9780857094940.79.
[28] Giasin K, Hodzic A, Phadnis V, Ayvar-Soberanis S. Assessment of cutting forces and hole quality in drilling Al2024 aluminium alloy: experimental and finite element study. Int J Adv Manuf Technol 2016;87:2041–61. https://doi.org/10.1007/s00170-016-8563-y.
[29] Ramya Devi G, Palanikumar K. Analysis on drilling of woven glass fibre reinforced aluminium sandwich laminates. J Mater Res Technol 2019;8:1024–35. https://doi.org/10.1016/j.jmrt.2018.06.021.
[30] Luo H, Fu J, Wu T, Chen N, Li H. Numerical Simulation and Experimental Study on the Drilling Process of 7075-t6 Aerospace Aluminum Alloy. Mater 2021;14. https://doi.org/10.3390/ma14030553.
[31] Ucun İ. 3D finite element modelling of drilling process of $_{Al7}$075-T6 alloy and experimental validation. J Mech Sci Technol 2016;30:1843–50. https://doi.org/10.1007/s12206-016-0341-0.
[32] Özel T. Computational modelling of 3D turning: Influence of edge micro-geometry on forces, stresses, friction and tool wear in PcBN tooling. J Mater Process Technol 2009;209:5167–77. https://doi.org/10.1016/j.jmatprotec.2009.03.002.
[33] Paktinat H, Amini S. Ultrasonic assistance in drilling: FEM analysis and experimental approaches. Int J Adv Manuf Technol 2017;92:2653–65. https://doi.org/10.1007/s00170-017-0285-2.
[34] Thepsonthi T, Özel T. 3-D finite element process simulation of micro-end milling Ti-6Al-4V titanium alloy: Experimental validations on chip flow and tool wear. J Mater Process Technol 2015;221:128–45. https://doi.org/10.1016/j.jmatprotec.2015.02.019.
[35] Lotfi M, Amini S. Experimental and numerical study of ultrasonically-assisted drilling. Ultrasonics 2017;75:185–93. https://doi.org/10.1016/j.ultras.2016.11.009.

Supplementary Files

This is a list of supplementary files associated with this preprint. Click to download.

- SUPPLEMENTARYDATA.docx
- floatimage1.jpeg